



HIGH-TEMPERATURE PHASES AND PROCESSES FOR ENABLING CLEANER PRODUCTION OF METALS AND ENERGY

Effect of Aluminizing on the Fatigue and High-Temperature Corrosion Resistance of Inconel 740 Nickel Alloy

IZABELA BARWINSKA ^{1,2} MATEUSZ KOPEC ^{1,3,5}
DOMINIK KUKLA ¹ MAGDALENA ŁAZIŃSKA ² RYSZARD SITEK ⁴
and ZBIGNIEW L. KOWALEWSKI ¹

1.—Institute of Fundamental Technological Research, Polish Academy of Sciences, Pawińskiego 5B, 02-106 Warsaw, Poland. 2.—Faculty of Advanced Technologies and Chemistry, Military University of Technology, 00-908, Warsaw, Poland. 3.—Department of Mechanical Engineering, Imperial College London, London SW7 2AZ, UK. 4.—Faculty of Materials Science and Engineering, Warsaw University of Technology, Wołoska 141, 02-507 Warsaw, Poland. 5.—e-mail: mkopec@ippt.pan.pl

The fatigue response and high-temperature corrosion resistance of Inconel 740 nickel alloy in its as-received state, and the same material with aluminized surface layer, were investigated. The aluminized layer was applied by using the chemical vapor deposition process with the participation of AlCl_3 vapors under a hydrogen protective atmosphere at a temperature of 1040°C for 8 h and internal pressure of 150 hPa. The microstructure of the aluminized layer was characterized through scanning electron microscopy and x-ray energy dispersive spectroscopy analysis. It was found that Inconel 740 with an aluminized surface exhibited an improved hardness and fatigue response of 100 MPa in the whole range of stress amplitudes from 350 MPa to 650 MPa. Additionally, the application of the aluminization process enhanced service life as well as the corrosion resistance of the alloy in question and effectively protected it against high-temperature corrosion.

INTRODUCTION

Materials for the turbine blades in aero-engines are exposed to high temperature, thus the alloys used in such applications should possess outstanding hot corrosion and oxidation resistance.¹ Another sector in which structural materials operate under high temperature and increased pressure is the power energy industry, commonly powered by fossil coal. The continuous development in this industry is aiming to reduce CO_2 emissions; however, it simultaneously leads to an increase in the temperature and pressure during power plant operation. The current operating temperature in power plants reaches up to 760°C , while the pressure generated could be as high as 35 MPa.² Such extreme conditions significantly reduce the number of materials that can be used.³ These materials must be characterized by excellent oxidation resistance, microstructural

stability, and adequate creep resistance during harsh service conditions.⁴ It is known that nickel-based superalloys are characterized by excellent mechanical properties, even under extreme conditions, due to their two-phase microstructure and their complex chemical composition.⁵ Among the nickel alloys, the precipitation-hardened Inconel 740 is known for its high creep strength and corrosion resistance. One should note that during creep at a temperature of $700\text{--}800^\circ\text{C}$, γ -austenitic phase and formation of the so-called lower carbides M_{23}C_6 could be observed. Inconel 740 has been developed for advanced ultra-supercritical steam boilers and it is mainly used for such purposes.⁶ Although it is characterized by excellent oxidation resistance, the microstructural changes observed during high-temperature exposure on the surface layer could significantly reduce its strength properties, including tensile strength and hardness.⁷ Oxidation of the Inconel 740H alloy leads to the formation of hard internal oxide particles and simultaneous reduction in the extent of the ductile γ' phase, which consequently contributes to a decrease in creep strength and limited crack resistance.^{4,6,7}

(Received October 13, 2022; accepted December 16, 2022; published online January 19, 2023)

Components operating at high temperature are particularly exposed to oxidation and degradation under corrosive environmental conditions; thus, aluminide coatings are commonly used to protect them from damage during operation.⁸ In order to further increase the corrosion resistance, a high aluminum content is applied to the surface by means of several methods including hot dip aluminizing coating, pack cementation, physical vapor deposition (PVD), and chemical vapor deposition (CVD).⁹ One should mention that for the proper protection of jet engine elements, diffusion aluminide coatings are the most commonly used.¹⁰ They are produced by high-temperature chemical processes during which the aluminum diffuses into the alloy surface, and then reacts with it to form a nickel aluminide coating. Aluminum oxidizes at high temperature and forms a thin and dense alumina scale, acting as a diffusion barrier that protects the substrate from rapid degradation.¹¹ Although the diffusion aluminizing processes, such as the cementation process, are efficient in terms of performance and cost, they are not conventionally used as they do not meet environmental standards.^{9–12} Therefore, the protective coating of modern turbine blades against corrosion at 700–950°C is applied primarily by the CVD method. The CVD method offers high repeatability, coating uniformity, excellent adhesion strength, and could be heat treated in a reaction chamber.¹⁰ The research conducted by Yavorska et al.¹³ on aluminum coatings obtained by using the CVD method confirms that they increase oxidation resistance significantly. In this study, the aluminide coating was deposited by low-activity CVD at 760°C and 1050°C for 4 h and 8 h, respectively, on two cylindrical samples made of Inconel 713LC. Such a process was followed by an oxidation test in an air atmosphere for 100 h at 1050°C. The results show that an extended deposition time at a higher temperature leads to the production of a coating that effectively reduces oxygen diffusion and successfully protects the substrate from further oxidation. Another study performed by Zagula-Yavorska et al.,¹⁴ in which coating was applied to Inconel 625 by the CVD method, confirms that aluminide coatings improve oxidation resistance significantly at a temperature of 1100°C, as they prevent the formation of growing Cr₂O₃ oxides. The detailed research conducted by Pytel et al.,¹⁵ in which the properties of coatings deposited on Inconel 100 by different methods were compared, showed that the thickness and oxidation resistance of the coating depends on the application process. In this study, the coatings were deposited on the substrate by using CVD, vapor phase aluminide (VPA), and out-of-pack method. The results demonstrated that the CVD coating is not only the thinnest but also has the highest resistance to cyclic oxidation at 1100°C. Furthermore, Kopec et al.¹⁶ reported that aluminide coating enhances the mechanical properties of nickel superalloy. It was

found that an aluminized layer deposited on MAR 247 by a low-activity CVD process improved the high temperature fatigue response significantly in comparison to that of the as-received material. Similar work was reported by Obrtlik et al.¹⁷ where the Inconel 713LC in the as-received state, and with aluminide coating, was subjected to a fatigue test at 800°C. It was concluded that the application of a diffusion coating has a beneficial effect on the fatigue life in the Manson–Coffin representation.

Since aluminide coatings applied by CVD increase the oxidation resistance of the substrate material,¹⁶ and could potentially enhance the fatigue response of nickel-based superalloys, the main aim of this research was to assess the suitability of such a method for Inconel 740. The as-received and aluminized Inconel 740 was subjected to fatigue testing and hardness measurements first. Subsequent fracture surface analysis was carried out to determine the failure mechanism. Secondly, high-temperature corrosion and its mechanisms for both these materials were assessed during long-time annealing for 100 h at 1000°C and further described by using detailed EDS mapping. The oxidation resistance effectiveness of the CVD coating was also analyzed through the comparison of relative weight gain for the as-received and aluminized Inconel 740 after such long-time exposure.

MATERIALS AND METHODS

Material Characterization

Inconel 740, with the chemical composition presented in Table I, was investigated in this research. The specimens were firstly machined in a computer numerical control (CNC) lathe machine to ensure a surface finish. Then, they were subjected to the aluminizing process (Fig. 1a) performed by using an IonBond apparatus and CVD process, with the participation of AlCl₃ vapors in a hydrogen atmosphere (carrier gas), at a temperature of 1040°C for 8 h, and a reduced pressure of 150 hPa. The process parameters were optimized prior to this study.

Mechanical Testing

Fatigue tests were performed on the MTS 858 testing machine, with an axial force range of ± 25 kN. The fatigue tests were force-controlled with zero mean level and a constant stress amplitude with a frequency of 20 Hz in the range of stress amplitude from ± 350 MPa to ± 650 MPa. The range of fatigue loads was established on the basis of the yield strength R_{0.2} determined from the uniaxial tensile test. Three specimens per stress amplitude were used to ensure the repeatability of tests. The geometry of the fatigue specimen is presented in Fig. 1b. Microhardness measurements were performed by means of the Vickers method on a Shimadzu HMV-G hardness tester using a loading force of 980.7 mN for a dwell time of 10 s.

Table I. Chemical composition of Inconel 740 in the as-received state

Element	Al	Nb	Ti	Fe	C	Mn	Si	Cr	Co	Ni
Wt.%	00.90	02.00	01.80	00.60	00.03	00.25	00.40	24.66	20.12	Bal

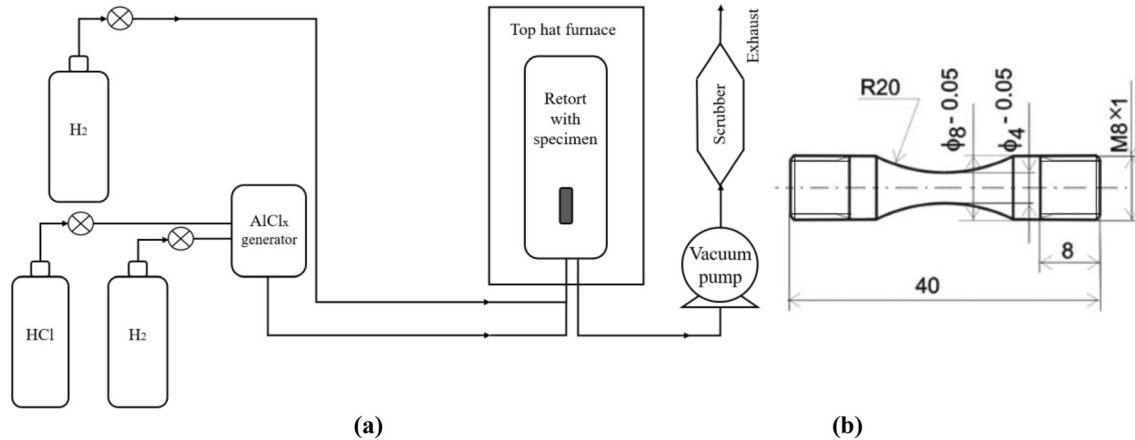


Fig. 1. (a) Scheme of the CVD process reaction chamber; (b) engineering drawing of the specimen for fatigue testing.

High-Temperature Oxidation

Five aluminized and five as-received specimens in the form of $5 \text{ mm} \times 5 \text{ mm} \times 2 \text{ mm}$ cuboids with an initial weight of 1.5 g were subjected to the heat resistance test at 1000°C for 100 h in an air atmosphere. Each specific specimen was removed from the furnace after 1 h, 5 h, 25 h, 50 h, and 100 h in order to measure its weight and dimensions by applying a precise micrometer screw gauge and laboratory scale, respectively. Oxidation kinetics was determined by mass gain and measurements of the scale after a specific time of the heat treatment.

Microstructural Observations

In the next step, the microstructural analysis was performed by using a Quanta 3D FEG field emission scanning electron microscope (SEM) operated at 20 kV with an EDS detector. Such a detector was also used to perform a qualitative chemical composition analysis. The effect of the heat treatment scale of the specimen on its surface for modified and unmodified sections was analyzed on grounded and mechanically polished cross-sections using SEM. The specimens for microstructural characterization were prepared by conventional metallographic procedures including hot mounting, grinding, and polishing. After mounting, the specimens were ground by using a Struers® polishing machine and 600, 800, 1200, 2400, and 4000 SiC graded papers. The polishing was carried out by means of Metrep® Durasilk M cloth, $3\text{-}\mu\text{m}$ diamond polishing solution and water-based lubricant.

RESULTS AND DISCUSSION

Microstructural Characterization of Aluminized Layers

Figure 2a shows the obtained uniform coating of approximately $25 \pm 2 \mu\text{m}$ thickness on the substrate material, produced by using the aluminizing process. The cross-sectional micrograph of the aluminide coating revealed the presence of three zones for the CVD process: an outer NiAl coating, the interdiffusion zone (IDZ), and the substrate material. The crack observed between the IDZ and outer NiAl coating occurred during the metallographic preparation of the specimen. The microscopic observations showed that the thickness of the outer NiAl layer was approximately $12 \mu\text{m}$. Below, a continuous and bright $8\text{-}\mu\text{m}$ -thick IDZ sub-layer, consisting of β -NiAl phase and carbides, could be clearly observed. The characteristic morphology for the deposition of diffusion aluminide coatings on the surface is illustrated in Fig. 2b and c. It consists of a “wave-like” AlNi structure with well-formed bumps formed and raised in a perpendicular direction to the surface.¹⁰

Effect of Aluminizing on Fatigue Response and Microhardness Profile of Inconel 740

The microhardness measurements of the substrate material and individual aluminide coating zones of the Inconel 740 are presented in Fig. 3a. The hardness of the as-received Inconel 740 was equal to 350 HV0.1. The outer coating was characterized by a hardness of 639 HV0.1, which was

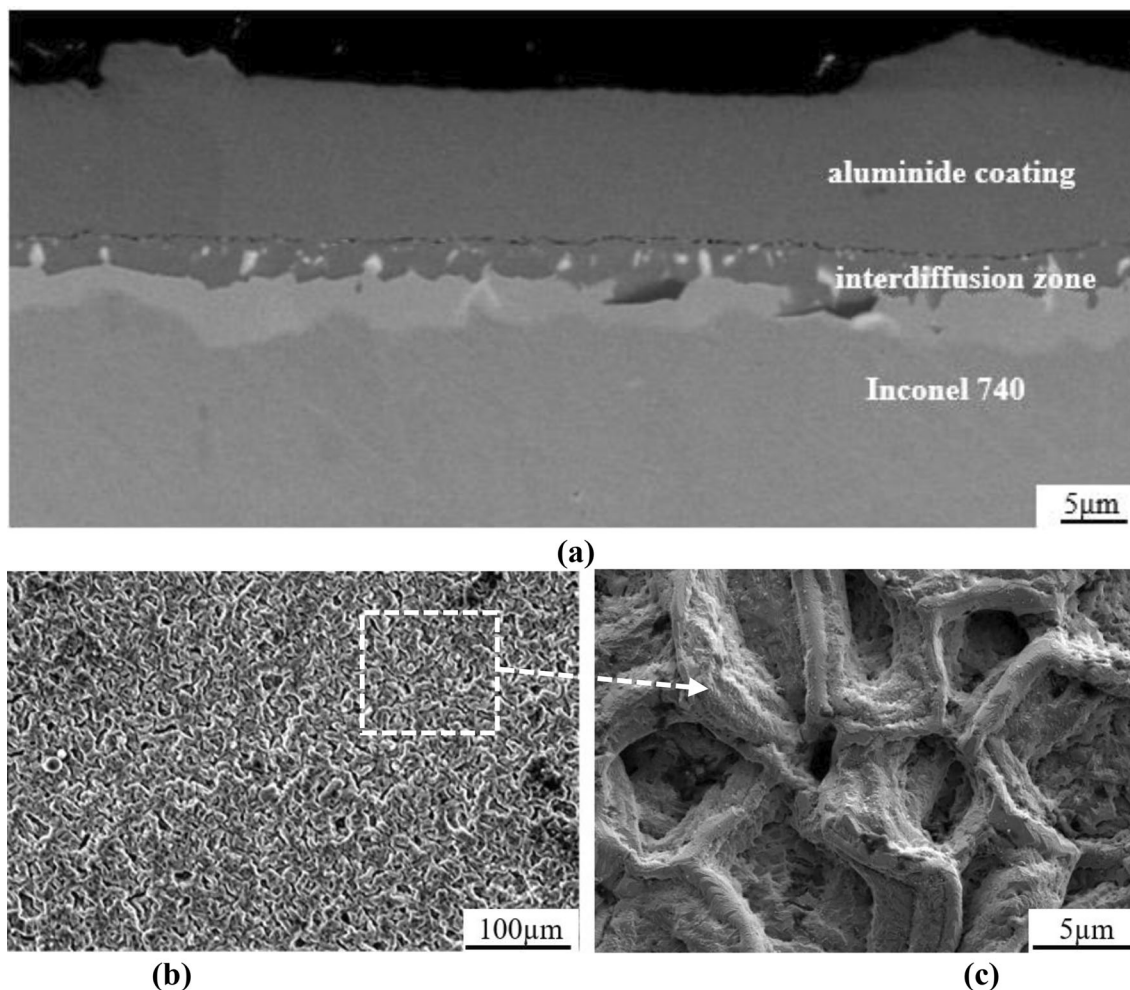


Fig. 2. (a) The cross-section of aluminized Inconel 740; (b, c) surface morphology of aluminized Inconel 740 surface.

ascribed to the aluminum atoms distributed in the lattice of the AlNi coating. The significant improvement in hardness could also be associated with the formation of AlNi phases during the high-temperature CVD process. The maximum hardness, as high as 780 HV0.1, occurred in the interdiffusion area where chromium, molybdenum, and cobalt carbides were dominant. The occurrence of such carbides reinforces the solution strengthening and, simultaneously, improves the hardness of the material.¹⁸

The effect of aluminizing on the mechanical properties of the Inconel 740 was also investigated during standard fatigue testing. Such tests were performed at a room temperature of 23°C. These feasibility studies provide insights into the deformation behavior of aluminized Inconel 740 and reveal the behavior of brittle coating subjected to cyclic loading. The experimental results showed that the aluminizing process improves the stress response of the Inconel 740 specimens by 100 MPa in the whole range of stress amplitudes from 350 MPa to 650 MPa (Fig. 3b). It should be mentioned that the fatigue response of aluminized

Inconel alloys at room temperature is similar or slightly lower than the as-received material, as reported for Inconel 714LC¹⁹ or MAR247.^{20,21} One should point out that during fatigue damage development, micro-voids are firstly initiated in the heavily precipitated interdiffusion zone of the coating by decohesion of the precipitate from the intermetallic matrix interface.²² Subsequently, the coalescence of micro-voids results in the formation of microcracks, and further failure propagates across the coating thickness. Since the interdiffusion zone of the aluminized Inconel 740 is relatively thick (Fig. 2a), the coating might improve the strength characteristics of the coated alloy in question and extend its service life significantly. The comparison of the number of cycles to failure for the same values of stress amplitude for as-received and aluminized Inconel 740 revealed a notable increase of service life with a simultaneous decrease of stress amplitude (Fig. 3c). Aluminized Inconel 740 exhibited a significant increase in service life from 260% to 430% with a simultaneous decrease of stress amplitude from 550 MPa to 450 MPa in comparison

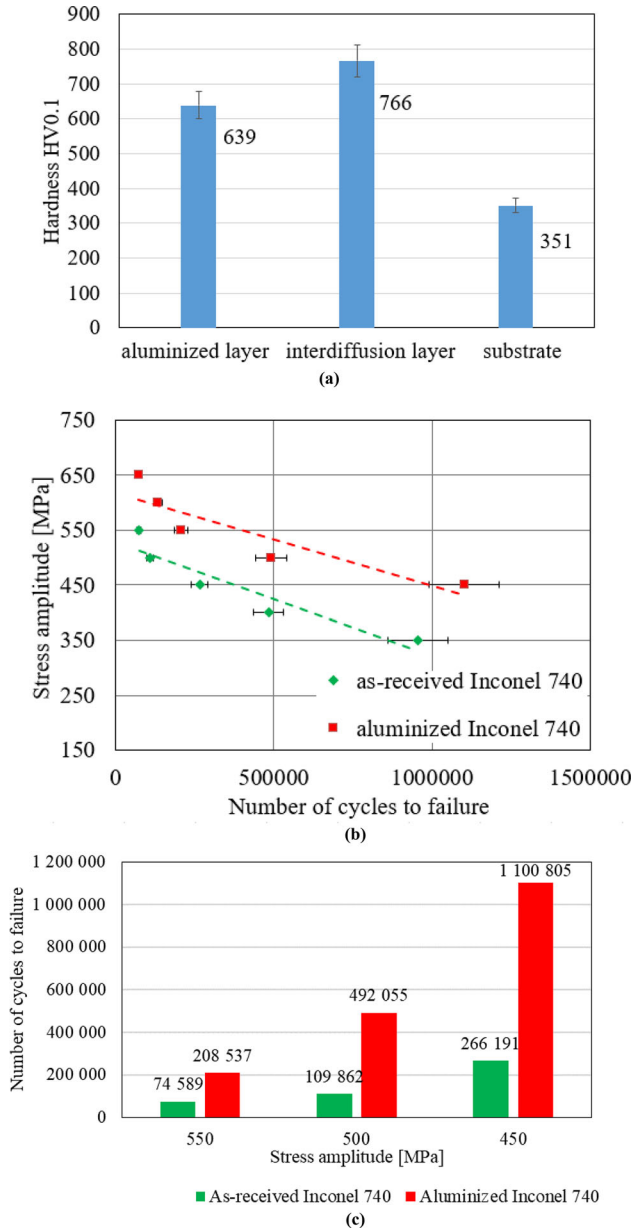


Fig. 3. (a) Microhardness of the aluminumized Inconel 740; (b) the S–N curve for Inconel 740 under different surface conditions; (c) the comparison of the number of cycles to failure for the defined stress amplitude.

to the as-received material. A recent publication²³ confirmed the suitability of the aluminumization process for the life enhancement of the nozzle guide vane of an aero gas turbine engine. In this paper, the coated vanes were evaluated through engine-level tests to assess their performance and durability. The engine level tests and subsequent inspection post accelerated emission test cycles ensured that the aluminumized vanes could withstand severe engine operating cycles without any damage or failure, which was not possible for uncoated parts.²³

Micrographs of the fatigue fracture surface of the aluminumized Inconel 740 are presented in Fig. 4.

Characteristic fracture surface morphologies were observed for all aluminumized specimens: an initiation area with radial streaks along the crack propagation direction and a relatively flat surface (marked as I in Fig. 4a and c), a propagation area with microvoids and dimples (marked as II in Fig. 4b and d), and an instantaneous fracture area (marked as III). A morphologically and dimensionally homogeneous layer of adhesive nature obtained in the CVD process can be observed in Fig. 4e. One can deduce that an improved strength response during fatigue testing might be attributed to the successfully performed CVD process and the stiff and hard coating formed. Crack initiation was mainly observed in the peripheral regions, at the edge of the specimen where the highest stress concentration occurred and the sub-surface defects could be found (Fig. 4c and e). The propagation area, characterized by microvoids, also contained microcracks formed due to jointing pores (Fig. 4f).

Effect of Aluminumizing on the Oxidation Behavior of Inconel 740

Surface morphology analysis was used first to investigate the oxidation process. The SEM images of representative specimens in the as-received and aluminumized state after 1 h of oxidation at 1000°C are illustrated in Fig. 5a, b, c and d. The surface of the as-received Inconel 740 was covered by fine (10–30 μm) precipitations of Cr₂O₃ oxides. From a thermodynamic point of view, titanium is more susceptible to the formation of oxides than chromium. However, the content of titanium in Inconel 740 is much lower, thus the formation of chromium oxides was mainly observed. On the other hand, the surface of the aluminumized specimen after oxidation was mainly characterized by fine TiO₂ precipitations, which may suggest a slower oxidation process and, thus, an inhibited growth of Cr₂O₃ oxides. Figure 5 presents the surface of the as-received (Fig. 5e and f) and coated specimen (Fig. 5g and h) after 50 h of oxidation. The extended high-temperature exposure causes the further formation of the external chromium scale and fine particles of titanium oxide on the uncoated specimen. Moreover, the oxidized surface of the coated specimen mainly consisted of aluminum oxide; however, nickel diffusion led to the appearance of NiAl phase at the grain boundaries.²⁴

Further oxidation at a temperature of 1000°C for 100 h led to the formation of a thin layer of NiCr₂O₄ (Fig. 5i and j). The formation of spinels was associated with the growth of a Cr₂O₃ outer layer. The longer heating time caused the diffusion of the chromium to the surface, and thus its depletion in the subsurface zone. As nickel has predominantly a high chemical concentration in the alloy, it began to diffuse into the surface layer, which subsequently led to the formation of NiCr₂O₄, as described in Ref. 25. Figure 5k and l presents an aluminumized surface

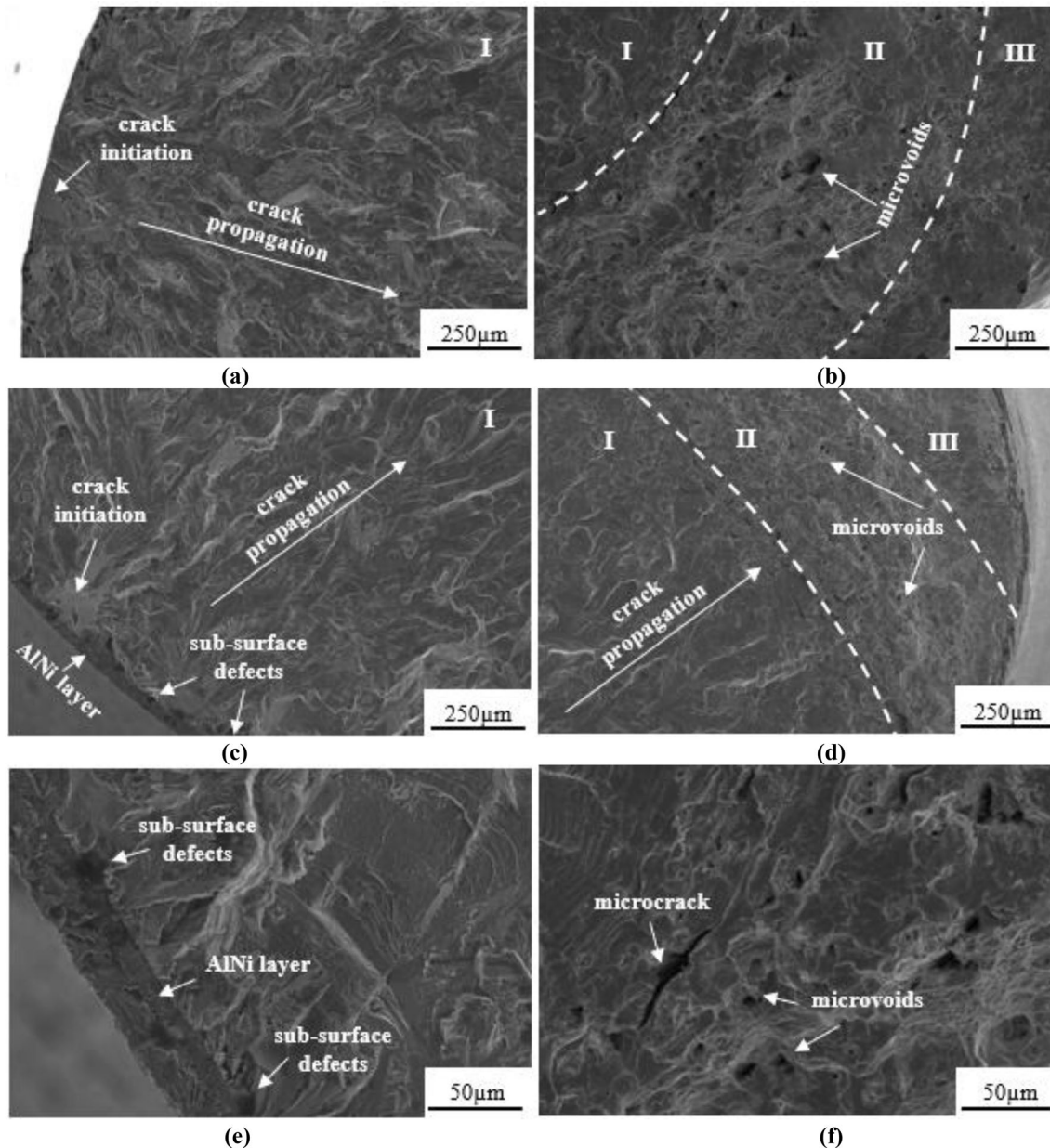


Fig. 4. (a, b) The as-received and (c–f) aluminized Inconel 740 fatigue fracture surfaces for a stress amplitude equal to 500 MPa.

of uniform and dense coating. The adherent and crack-free layer was composed of randomly scattered globular nodules.

In order to accurately assess the development of the oxidation at 1000°C with respect to the high-temperature exposure time, both the as-received and aluminized Inconel 740 cross-sections were analyzed after specific time ranges. The coated specimen that was 25 μm thick was characterized by an increased content of aluminum near the surface (Fig. 6a, Table II). The aluminum, titanium, and niobium enriched IDZ of approximately 8 μm separates the coating from the diffusion zone of 15 μm, in which a considerable content of chromium could be found. The chemical composition is

stable and close to the as-received condition approximately 35 μm from the IDZ. On the other hand, the uncoated specimen was covered by approximately 4 μm of chromium-enriched scale (Fig. 6b). The high temperature led to the formation of a diffusion zone of approximately 17 μm in which an increased content of cobalt could be observed (Table II). Moreover, aluminum and niobium-rich areas were found close to the specimen surface.

The extension of the high-temperature exposure time resulted in a slight increase of the diffusion zone for the coated Inconel 740 from 15 μm to 25 μm. The segregation of the main elements can be clearly observed in EDS maps (Fig. 6c). The aluminum remained on the top part of the coating,

while niobium, chromium, titanium, and manganese diffused to the IDZ. One should note that an annealing time of up to 50 h significantly affected the thickness of the chromium oxide layer of the uncoated specimen. Such a long high-temperature exposure time results in the layer thickness increasing from 4 μm to 8 μm (Fig. 6d) in comparison to the case of 1 h (Fig. 6c). A relatively long time of annealing led to the further diffusion of aluminum atoms to the surface, with 9% measured near the top surface, 3% in the IDZ, and 2% just below it (Table II). One should notice that the

thickness of the diffusion zone increased from 15 μm to 27 μm .

Similar observations were performed by Nowak et al.²⁶ who studied the oxidation resistance of aluminized Inconel 625 and Inconel 738 nickel alloys during thermal shock at 1120°C. The test consisted of heating the sample for 2 h, and then cooling it for 15 min using compressed air. This process was repeated for 200 cycles. The results showed that the surface of samples after the oxidation process was characterized by a scale rich in aluminum and oxygen, which indicates the formation of Al_2O_3 and the depletion of the core in

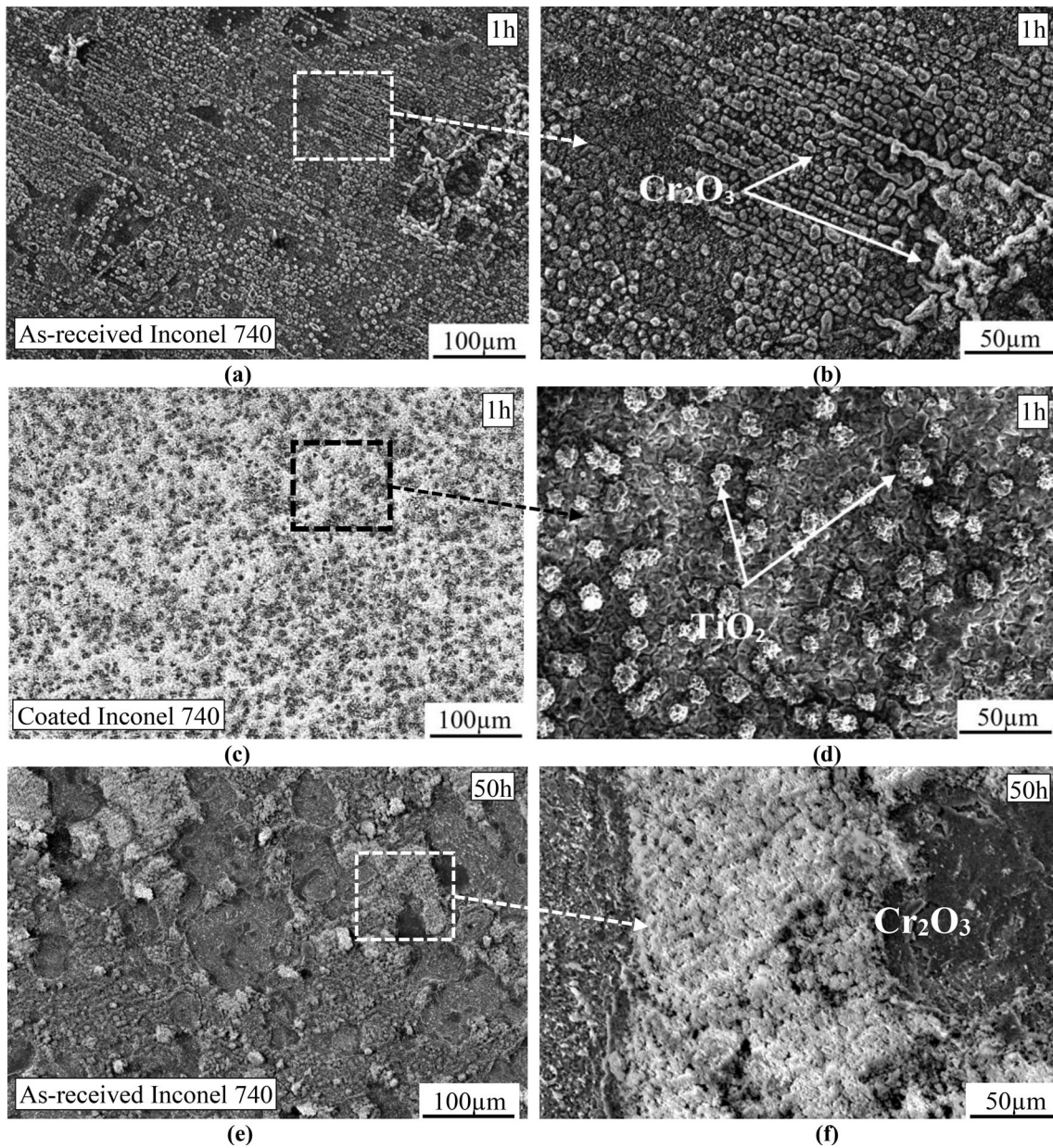


Fig. 5. The surface morphology of (a, b) as-received Inconel 740 and (c, d) aluminized Inconel 740 after (e, f) 1 h exposure at 1000°C; (g, h) as-received Inconel 740 and aluminized Inconel 740 after 50 h exposure at 1000°C; (i, j) as-received Inconel 740 and (k, l) aluminized Inconel 740 after 100 h exposure at 1000°C.

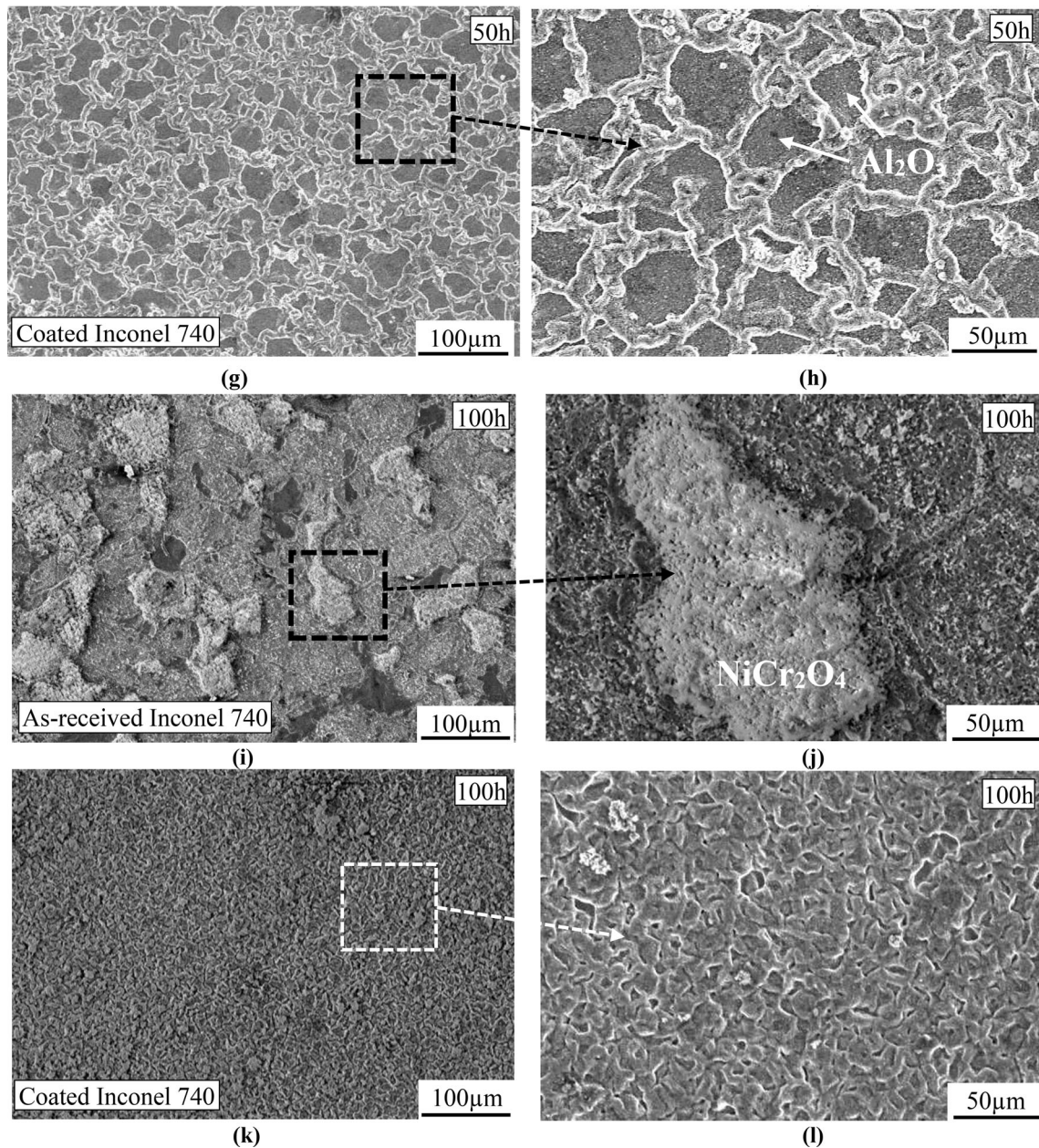


Fig. 5. continued.

the aluminum. Additionally, the dissolution of the IDZ zone was also noticed under the influence of the high temperature of the process and the reduced content of aluminum.

The final extension of the homogenization time from 50 h up to 100 h did not affect the structure of the coated specimen (Fig. 7a). The content of the alloying elements remained similar with the aluminum oxide on top of the coating (Table II—point 8, Table III—point 1) and niobium, titanium and chromium enriched IDZ (Table II—point 9, Table III—point 2). The observations of the uncoated specimen revealed a significant increase in the chromium oxide thickness to 15 μm and a total increase of the thickness over the entire zone by

430% in comparison to the thickness measured after 1 h of annealing. A significant content of chromium (71.75%) and oxide (26.57%) could be found in the formed scale. The diffusion of nickel was successfully inhibited by the chromium oxide sublayer; however, the diffusion zone grew considerably to approximately 50 μm (Fig. 7b). One can conclude that the formation of protective chromium oxide restrains the outward diffusion of alloy elements and reduces the activity of oxygen at the alloy scale.⁴ Such behavior enables the stabilization of the oxidation process to a relatively steady state. The observations of the oxidation kinetics of uncoated Inconel 740 reveal both the continuous growth of chromium oxide, from 4 μm after 1 h of annealing to approximately 13 μm

after 100 h, and a significant increase of the width of the diffusion zone beneath it from 15 μm to 50 μm . The mechanism of element diffusion remained the same, as chemically active aluminum is effectively inhibited below the scale. However, its limited content does not enable the formation of continuous scale and aluminum oxides grow as inner oxides.²⁷ The diffusion and subsequent oxidation kinetics are closely related to the temperature—the higher the temperature, the higher the diffusion rate of the alloy elements, and thus the formation of the oxide scale increases.⁴

The evolution of the relative weight gain and thickness of the oxidation scale versus the oxidation time up to 100 h at 1000°C for the as-received and aluminized Inconel 740 is presented in Fig. 8a and b, respectively. Both materials exhibited a mass

gain; however, their behavior is different. It can be observed that the as-received Inconel 740 lost its mass after 50 h, which was probably caused by the spallation of the oxide layer. Similar behavior was also reported by Chyrkin et al.²⁸ who observed the spallation of the oxide on 1-mm-thick alloy 625 oxidized at 1000°C under air. The spallation process was intensified during the specimen cooling and was associated with a high residual stress (greater than the ultimate tensile strength of the oxide). A similar spallation was also observed for aluminized Inconel 600 during isothermal oxidation tests performed at 1000°C for 6 h, 36 h, and 90 h.²⁴ On the other hand, aluminized Inconel 740 exhibited a great heat resistance as steady relative weight gain until 50 h of annealing, followed by its stabilization at around 0.2%. On the other hand, the evolution of

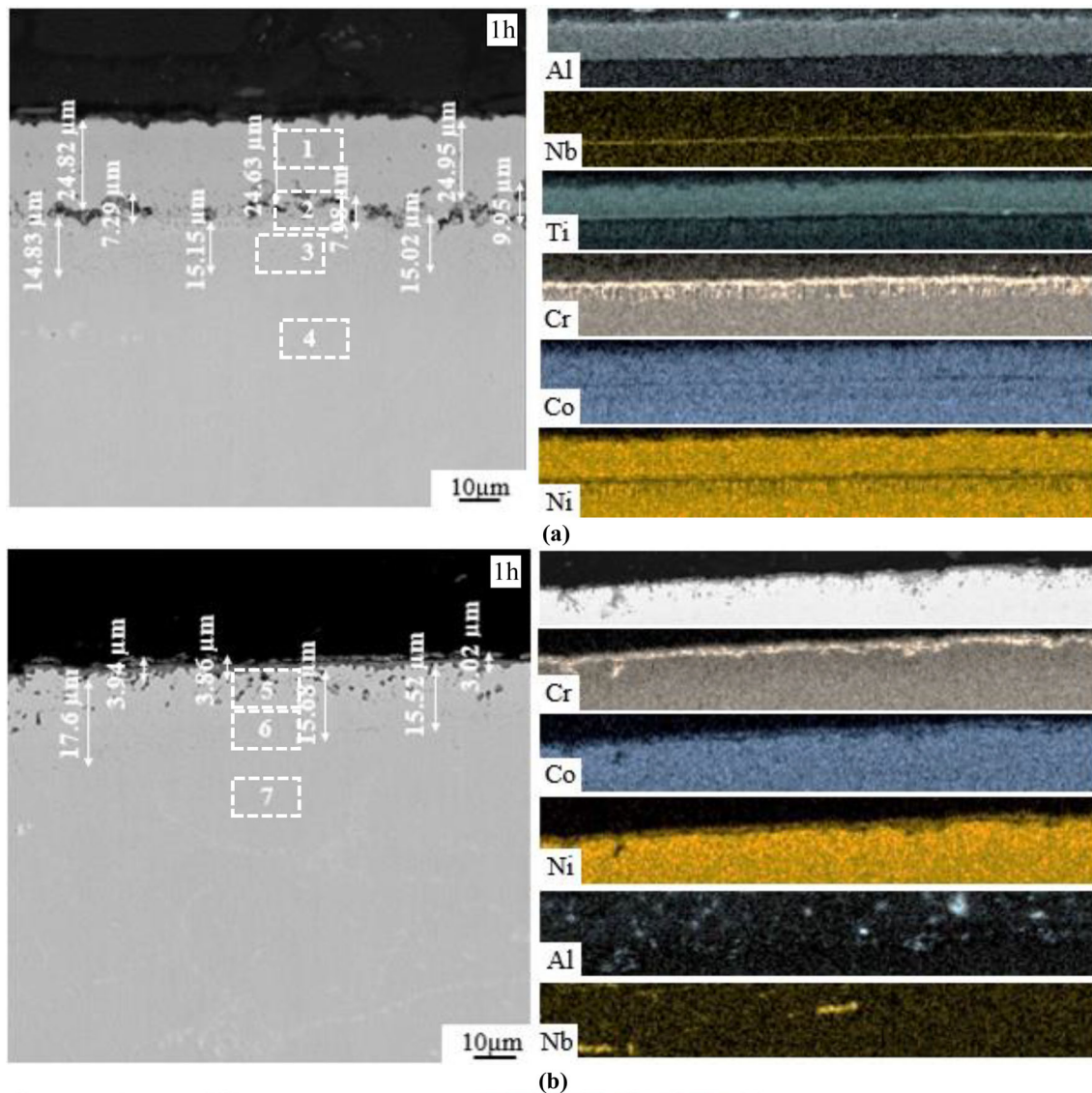


Fig. 6. The cross-section micrographs and EDS maps of (a) as-received Inconel 740 and (b) aluminized Inconel 740 after 1 h exposure at 1000°C and (c) as-received Inconel 740 and (d) aluminized Inconel 740 after 50 h exposure at 1000°C.

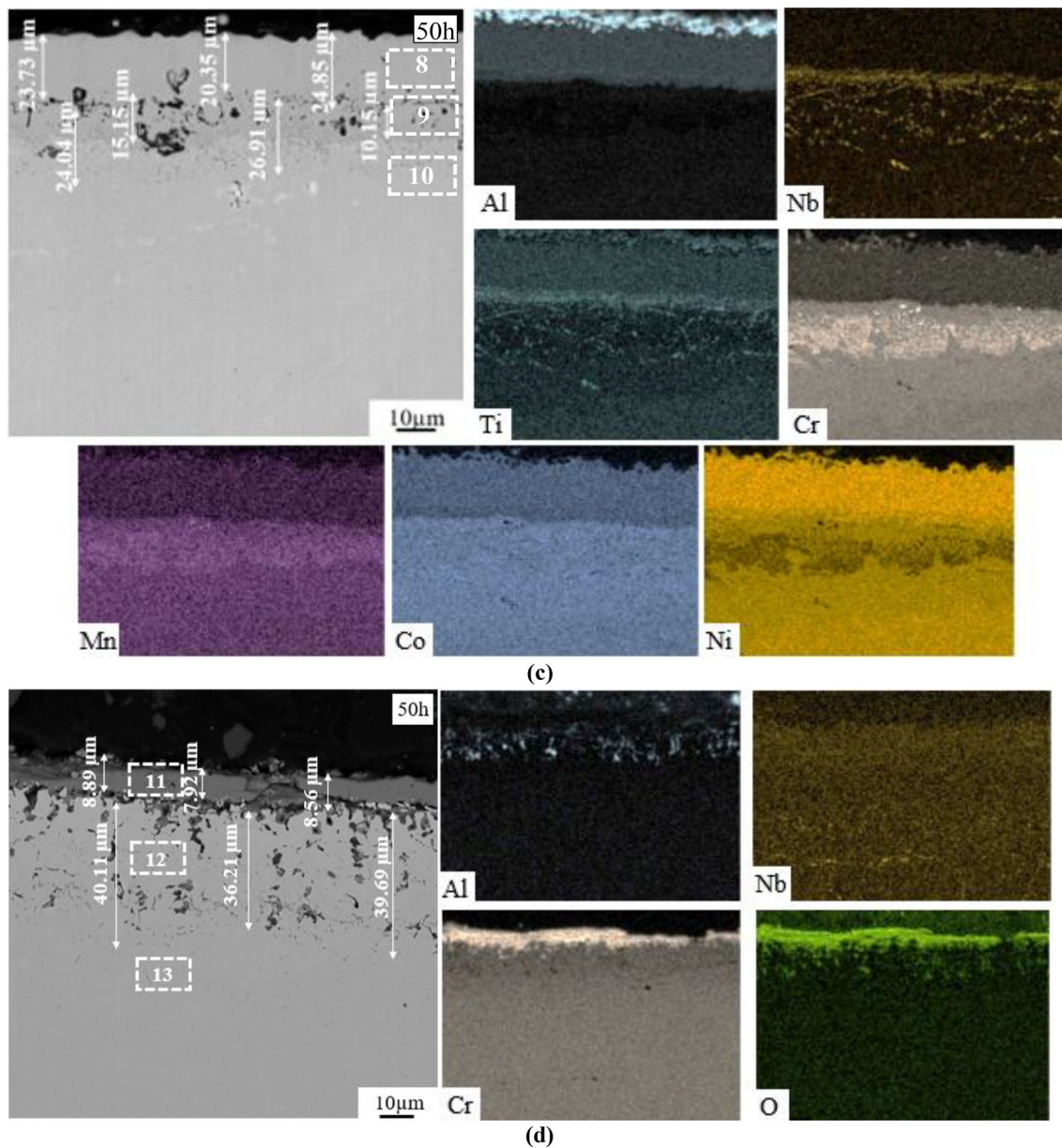


Fig. 6. continued.

oxide scale thickness presented in Fig. 8b revealed a significant improvement in terms of oxidation resistance for the coated Inconel 740. Aluminized alloy was characterized by a relatively low and stable increase in oxidation scale thickness during high-temperature annealing for up to 100 h. Remarkable changes were found in the uncoated alloy in which the oxidation scale grew from the very beginning of the annealing from 4 μm to 15 μm . The optimized CVD process enabled the application of a tight and well-adhered AlNi coating on Inconel 740. One can say that aluminization increases the heat resistance of Inconel 740 significantly, and thus could be successfully used to protect it against hot temperature corrosion.

CONCLUSION

In this research, the mechanical properties of the as-received and aluminized Inconel 740 alloy were compared and examined using standard fatigue tests and microhardness measurements. The aluminization of Inconel 740 enhanced its fatigue response by around 100 MPa in the whole range of stress amplitudes from 350 MPa to 650 MPa, and increased the hardness of the modified surface by 200%. Aluminized Inconel 740 exhibited a significant increase in service life from 260% to 430% with a simultaneous decrease of stress amplitude from 550 MPa to 450 MPa in comparison to the as-received material. Additionally, the application of the aluminizing process improved the corrosion

Table II. Chemical composition of the specific regions of the as-received Inconel 740 (1, 2, 3, 4) and aluminized material (5, 6, 7) after 1 h of annealing at 1000°C, and of the as-received Inconel 740 (7, 8, 9) and aluminized material (10, 11, 12, 13) after 50 h of annealing at 1000°C

Element	Ni	O	Al	Si	Nb	Ti	Cr	Co
1	48.46	–	13.30	–	–	17.58	02.94	17.99
2	43.66	04.07	14.80	01.54	05.10	17.08	–	10.65
3	17.90	–	00.72	01.27	02.98	06.07	50.26	20.78
4	51.31	–	00.94	00.67	02.05	01.08	23.01	20.23
5	59.29	–	–	00.50	01.49	00.40	14.97	23.38
6	51.68	05.98	03.18	00.43	01.27	–	13.13	20.45
7	53.72	–	00.57	00.54	01.38	01.31	21.19	21.28
8	44.80	–	09.00	00.48	00.72	01.40	20.50	23.10
9	41.51	–	03.21	00.48	05.40	08.32	20.49	20.68
10	43.40	–	02.33	00.60	06.74	02.95	23.48	20.89
11	–	22.64	–	–	–	01.99	75.38	–
12	59.18	–	01.94	00.48	–	00.29	13.59	24.51
13	51.28	–	00.86	00.57	01.18	01.62	23.58	20.91

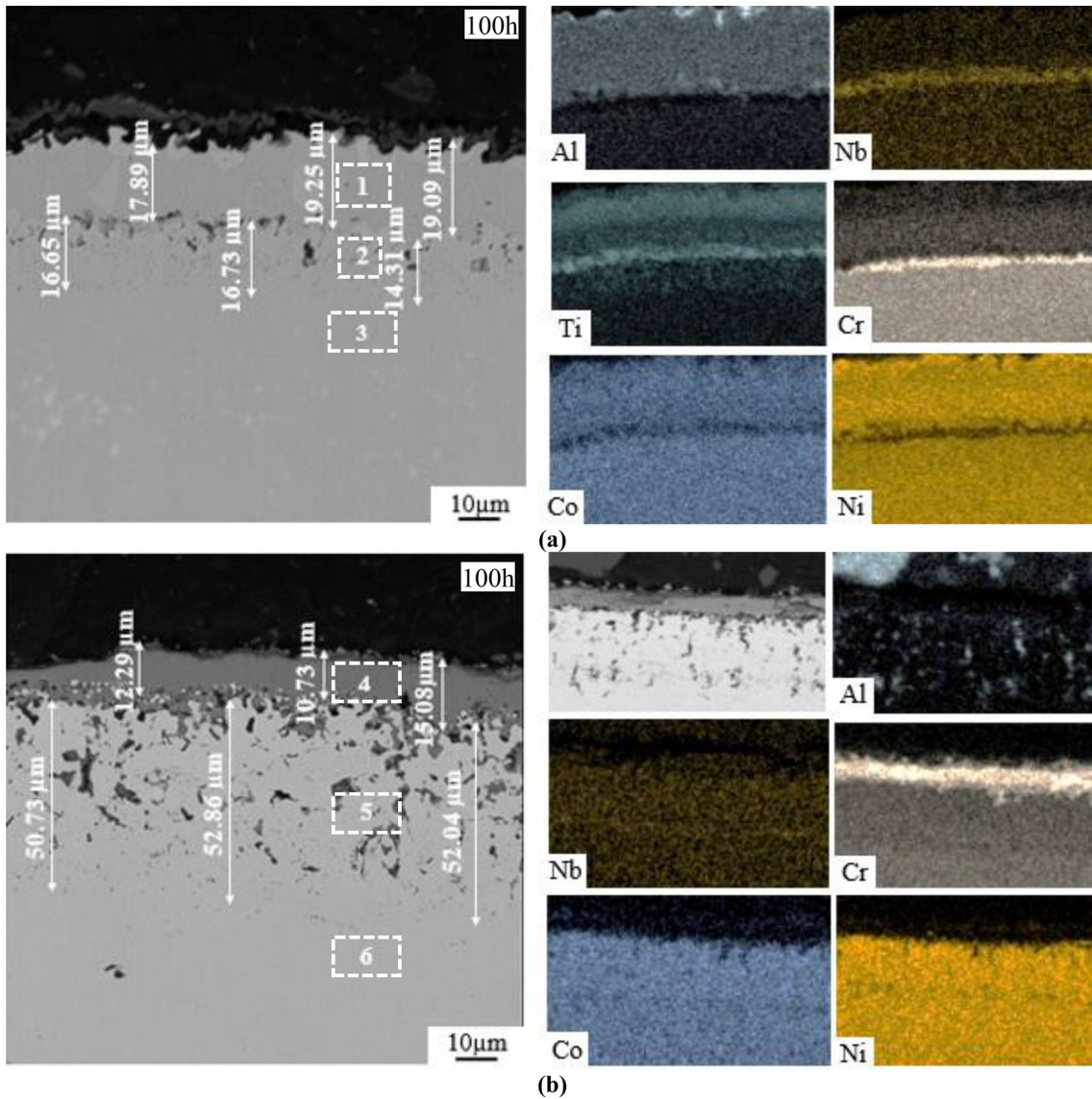


Fig. 7. The cross-section micrographs and EDS maps of (a) as-received Inconel 740 and (b) aluminized Inconel 740 after 100 h exposure at 1000°C.

Table III. Chemical composition of the specific regions of the as-received Inconel 740 (1, 2, 3) and aluminized material (4, 5, 6, 7) after 100 h annealing at 1000°C

Element	Ni	O	Al	Si	Nb	Ti	Cr	Co
1	49.74	–	04.06	00.50	00.73	01.38	20.55	23.05
2	41.63	–	03.09	00.43	05.35	08.43	20.38	20.68
3	43.40	–	02.37	00.57	06.89	02.80	23.28	20.69
4	–	26.57	–	–	–	01.68	71.75	–
5	59.98	–	01.30	00.44	01.21	–	12.24	24.83
6	52.82	–	00.82	00.51	01.37	01.47	22.22	20.80

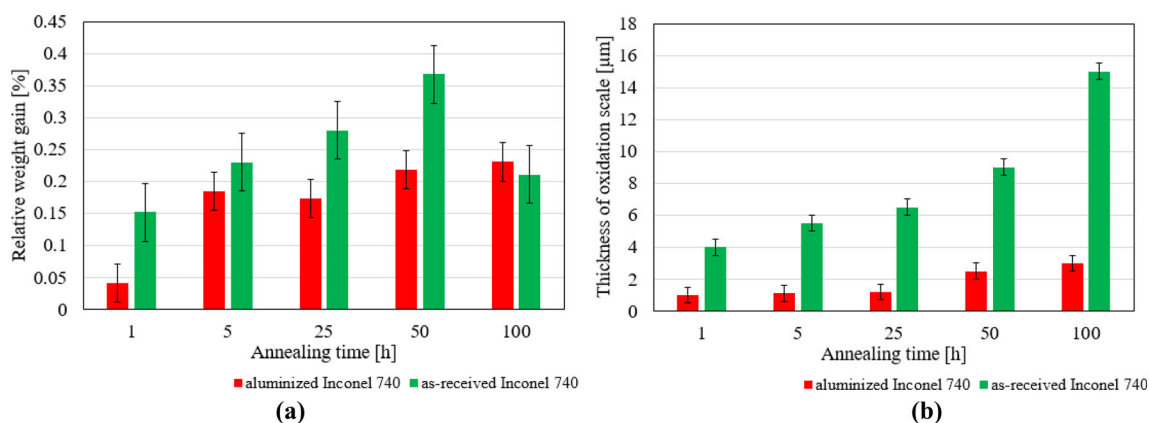


Fig. 8. (a) The comparison of relative weight gain and (b) thickness of oxidation scale for the as-received and aluminized Inconel 740 after long-time exposure at 1000°C.

resistance of Inconel 740 significantly, since the effective protection of its surface against high-temperature oxidation was successfully achieved. The stability of relative weight gain and thickness of the oxidation scale for the aluminized Inconel 740 corresponded to the stabilization of the aluminum oxide during the high-temperature annealing at 1000°C either for 50 h or 100 h. It was concluded that the aluminizing process improves the heat resistance of Inconel 740 remarkably, and therefore can be treated as a promising tool for protecting it against hot-temperature corrosion.

ACKNOWLEDGEMENTS

The author would like to express his gratitude to the technical staff—Mr M. Wyszowski and Mr A. Chojnacki for their kind help during the experimental part of this work.

CONFLICT OF INTEREST

The authors declare that they have no known competing financial interests or personal relationships that could have appeared to influence the work reported in this paper.

OPEN ACCESS

This article is licensed under a Creative Commons Attribution 4.0 International License, which per-

mits use, sharing, adaptation, distribution and reproduction in any medium or format, as long as you give appropriate credit to the original author(s) and the source, provide a link to the Creative Commons licence, and indicate if changes were made. The images or other third party material in this article are included in the article's Creative Commons licence, unless indicated otherwise in a credit line to the material. If material is not included in the article's Creative Commons licence and your intended use is not permitted by statutory regulation or exceeds the permitted use, you will need to obtain permission directly from the copyright holder. To view a copy of this licence, visit <http://creativecommons.org/licenses/by/4.0/>.

REFERENCES

1. A. Szczepankowski and R. Przysowa, *Eng. Fail. Anal.* <http://doi.org/10.1016/j.engfailanal.2022.106088.M> (2022).
2. X. Xie, Y. Wu, C. Chi, and M. Zhang, *Superalloys*, ed. M. Aliofkhaezrai (IntechOpen, London, 2015).
3. M. Grudziń-Rakoczy, Ł. Rakoczy, R. Cygan, F. Kromka, Z. Pirowski, and O. Milkovič, *Materials*. <https://doi.org/10.3390/ma13102362> (2020).
4. J. Lu, Z. Yang, S. Xu, H. Zhao, and Y. Gu, *HTMP*. <https://doi.org/10.1515/htmp-2014-0242> (2016).
5. M. Perrut, P. Caron, M. Thomas, and A. Couret, *C R Phys.* <https://doi.org/10.1016/j.crhy.2018.10.002> (2018).
6. J.J. de Barbadillo, B.A. Baker, R.D. Gollihue, and S.A. McCoy. *Properties of Inconel Alloy 740H for High Pressure Steam and Supercritical CO₂ Applications*. Paper presented at the ASME 2018 Symposium on Elevated Temperature

- Application of Materials for Fossil, Nuclear, and Petrochemical Industries, Seattle, Washington, USA, 2018. <https://doi.org/10.1115/ETAM2018-6741>.
7. A. Zieliński, M. Sroka, and T. Dudziak, *Materials*. <https://doi.org/10.3390/ma11112130> (2018).
 8. M. Goral, M. Pytel, K. Ochal, M. Drajewicz, T. Kubaszek, W. Simka, and L. Nieuzyła, *Coatings*. <https://doi.org/10.3390/coatings11040421> (2021).
 9. K.M. Döleker, A. Erdogan, T. Yener, A.C. Karaoglanlı, O. Uzun, M.S. Gök, and S. Zeytin, *Surf. Coat. Technol.* <https://doi.org/10.1016/j.surfcoat.2021.127069> (2021).
 10. S. Adamiak, W. Bochnowski, A. Dziedzic, R. Filip, and E. Szeregij, *HTMP*. <https://doi.org/10.1515/htmp-2014-0139> (2016).
 11. W. Szkliniarz, G. Moskal, A. Szkliniarz, and R. Swadźba, *Coatings*. <https://doi.org/10.3390/coatings8030113> (2018).
 12. V. Genova, L. Paglia, G. Pulci, C. Bartuli, and F. Marra, *Coatings*. <https://doi.org/10.3390/coatings11040412> (2021).
 13. M. Yavorska, J. Sieniawski, and M. Zielińska, *Arch. Metall. Mater.* <https://doi.org/10.2478/v10172-011-0022-z> (2011).
 14. M. Zagula-Yavorska, J. Sieniawski, R. Filip, and M. Drajewicz, *Solid State Phenom.* <https://doi.org/10.4028/www.scientific.net/SSP.227.313> (2015).
 15. M. Pytel, M. Góral, and M. Maliniak, *Arch. Mater. Sci. Eng.* 53, 102 (2012).
 16. M. Kopec, D. Kukla, X. Yuan, W. Rejmer, Z.L. Kowalewski, and C. Senderowski, *Coatings*. <https://doi.org/10.3390/coatings11010048> (2021).
 17. K. Obrtlík, S. Pospíšilová, M. Juliš, T. Podrábský, and J. Polák, *Int. J. Fatigue*. <https://doi.org/10.1016/j.ijfatigue.2011.12.010> (2012).
 18. M. Wang, B. You, Y. Wu, B. Liang, X. Gao, W. Li, and Q. Wei, *Metals*. <https://doi.org/10.3390/met12050735> (2022).
 19. K. Slámečka, J. Pokluda, M. Kianicová, J. Horníková, and K. Obrtlík, *Eng. Fract. Mech.* <https://doi.org/10.1016/j.engfractmech.2013.01.001> (2013).
 20. D. Kukla, M. Kopec, K. Wang, C. Senderowski, and Z.L. Kowalewski, *Materials*. <https://doi.org/10.3390/ma14143824> (2021).
 21. I. Šulák, K. Obrtlík, L. Čelko, P. Gejdoš, and D. Jech, *Adv. Mater. Sci. Eng.* <https://doi.org/10.1155/2018/9014975> (2018).
 22. M.K. Kumawat, R. Sarkar, V. Jayaram, and Md.Z. Alam, *Surf. Coat. Technol.* <https://doi.org/10.1016/j.surfcoat.2021.127787> (2021).
 23. R.K. Mishra, P. Kumar, K. Rajesh, C.R. Das, G. Sharma, and D.K. Srivastava, *Int. J. Turbo Jet Engines*. <https://doi.org/10.1515/tjj-2017-0050> (2021).
 24. T. Yener, K.M. Doleker, A. Erdogan, M. Oge, Y. Er, A.C. Karaoglanlı, and S. Zeytin, *Surf. Coat. Technol.* <https://doi.org/10.1016/j.surfcoat.2022.128295> (2022).
 25. H. Jiang, J. Dong, and M. Zhang, *Oxid. Met.* <https://doi.org/10.1007/s11085-015-9543-6> (2015).
 26. W.J. Nowak, K. Ochal, P. Wierzba, K. Gancarczyk, and B. Wierzba, *Metals*. <https://doi.org/10.3390/met9070782> (2019).
 27. S. Tang, S. Zhu, X. Tang, H. Pan, X. Chen, and Z.D. Xiang, *Corros. Sci.* <https://doi.org/10.1016/j.corsci.2013.11.054> (2014).
 28. A. Chyrkin, P. Huczowski, V. Shemet, L. Singheiser, and W.J. Quadackers, *Oxid. Met.* <https://doi.org/10.1007/s11085-010-9225-3> (2011).

Publisher's Note Springer Nature remains neutral with regard to jurisdictional claims in published maps and institutional affiliations.